Research Square

Preprints are preliminary reports that have not undergone peer review.
They should not be considered conclusive, used to inform clinical practice,
or referenced by the media as validated information.

Intratumoural immune heterogeneity as a hallmark of tumour evolution and progression in hepatocellular carcinoma

Phuong Nguyen
Translational Immunology Institute (TII), SingHealth-DukeNUS Academic Medical Centre, Singapore.
Siming Ma
Genome Institute of Singapore (GIS), Agency for Science, Technology and Research (A*STAR)
Cheryl Phua
Genome Institute of Singapore (GIS), Agency for Science, Technology and Research (A*STAR)
Neslihan KAYA
Genome Institute of Singapore (GIS), Agency for Science, Technology and Research (A*STAR)
Hannah Lai
Genome Institute of Singapore (GIS), Agency for Science, Technology and Research (A*STAR)
Chun Jye Lim
Institute of Molecular and Cell Biology
Jia Qi Lim
Genome Institute of Singapore (GIS), Agency for Science, Technology and Research (A*STAR)
Liyun Lai
Translational Immunology Institute (TII), SingHealth-DukeNUS Academic Medical Centre, Singapore.
Wai Leong Tam
Genome Institute of Singapore https://orcid.org/0000-0003-2365-5264
Kiat Hon Lim
Singapore General Hospital
Wei Keat Wan
Department of Pathology, Singapore General Hospital, Singapore
Tracy Loh
Department of Pathology, Singapore General Hospital, Singapore
Wei Qiang Leow
Department of Pathology, Singapore General Hospital, Singapore
Yin Huei Pang
National University of Singapore
Chung Yip Chan
Singapore General Hospital
Ser Yee Lee

Department of Hepatopancreatobiliary and Transplant Surgery, Singapore General Hospital, Singapore

Peng Chung Cheow

Department of Hepatopancreatobiliary and Transplant Surgery, Singapore General Hospital, Singapore

Han Chong Toh

NCCS

Florent Ginhoux

Singapore Immunology Network (SIgN), Agency for Science, Technology and Research (A*STAR) https://orcid.org/0000-0002-2857-7755

Shridhar Iyer

Division of Hepatobiliary & Pancreatic Surgery, National University Hospital Singapore

Alfred Kow

Division of Hepatobiliary & Pancreatic Surgery, National University Hospital Singapore

Yock Young Dan

Division of Gastroenterology and Hepatology, National University Hospital Singapore

Alexander Chung

SGH

Brian Goh

SGH

Salvatore Albani

Translational Immunology Institute https://orcid.org/0000-0002-5602-6256

Pierce Kah-Hoe Chow

Duke-NUS Medical School, Singapore & National Cancer Centre, Singapore & Department of Hepatopancreatobiliary and Transplant Surgery, Singapore General Hospital https://orcid.org/0000-0003-0584-2584

Wei Wei Zhai

Genome Institute of Singapore (GIS), Agency for Science, Technology and Research (A*STAR)

Valerie Chew (valerie.chew.s.p@singhealth.com.sg)

Translational Immunology Institute (TII), SingHealth-DukeNUS Academic Medical Centre, Singapore. https://orcid.org/0000-0002-5617-0936

Article

Keywords: Tumour evolution, immune microenvironment, tumour heterogeneity, immunoediting, immune suppression

Posted Date: July 22nd, 2020

DOI: https://doi.org/10.21203/rs.3.rs-41338/v1

License: This work is licensed under a Creative Commons Attribution 4.0 International License.
Read Full License

Version of Record: A version of this preprint was published at Nature Communications on January 11th, 2021. See the published version at https://doi.org/10.1038/s41467-020-20171-7.

Abstract

The clinical relevance of immune landscape intratumoural heterogeneity (immune-ITH) and its role in tumour evolution remain largely unexplored. Here, we uncovered significant spatial and phenotypic immune–ITH from multiple tumour sectors and deciphered its relationship with tumour evolution and disease progression in hepatocellular carcinomas (HCC). Immune–ITH was associated with RNA-ITH and distinct immune microenvironments. Tumours with low immune–ITH experienced higher immunoselective pressure and underwent escape mechanisms via loss of heterozygosity in human leukocyte antigens and immunoediting. Instead, the tumours with high immune-ITH were associated with a more immunosuppressive/exhausted microenvironment. This immune pressure gradient along with immune-ITH represents a hallmark of tumour evolution closely linked to the transcriptome-immune networks contributing to disease progression and immune inactivation. Remarkably, high immune-ITH and its transcriptomic signature were predictive for worse clinical outcome in HCC patients. This in-depth investigation of ITH provides novel evidence on tumour-immune co-evolution along HCC progression.

Introduction

Hepatocellular carcinoma (HCC) is known to be a heterogeneous tumour derived primarily from a background of chronic liver inflammation with various etiopathogenesis including chronic viral hepatitis infection, alcoholism and fatty liver diseases[1]. Due to the heterogenous nature of HCC and hence the limited options for targeted treatment, HCC remains the third leading cause of cancer mortality globally[2]. The recent success of immunotherapy in HCC benefit only up to 20% of the patients, who would respond to the anti-PD-1 checkpoint inhibitor monotherapy[3, 4]. Therefore, the current immunotherapy landscape leans towards combination therapy with enhanced clinical efficacy, such as that demonstrated by the recently approved atezolizumab (anti-PD-L1) and bevacizumab (anti-VEGFA) combination therapy in the phase III (IMbrave150) trial[5]. Moreover, a recent biomarker study from liver cancer patients treated with immune-checkpoint blockade demonstrated that low intratumoural transcriptomic diversity and cytolytic activity of CD8 + T cells predicts response to immunotherapy[6]. This warrants a deeper understanding of the complex nature of immune microenvironment and its relationship with tumour genomic profiles in a spatio-temporal manner.

The intratumoural heterogeneity (ITH) in the genomic landscape was previously described as an important hallmark of tumour evolution and cancer progression[7] including in HCC[8, 9]. On the flip side, the biological and clinical relevance of ITH in the tumour microenvironment (TME) based upon comprehensive immune profiling of the spatial distributions and the phenotypes of tumour-infiltrating leukocytes (TILs), remains unexplored. Recent multiomic analyses have explored and described intensive ITH in TME of HCC[10]. Other recent studies using immunogenomics approach addressed how the immune landscape contributes to genomic-ITH in ovarian cancer[11] and HCC[12]. Despite that, ITH on the immune landscape remains a correlative feature associated with tumour genomic-ITH and its direct clinical impact and role in tumour evolution unexplored. On the other hand, tumour evolution or immunoediting

driven by immunoselective pressure was previously demonstrated in other cancers[13, 14]. It is also not known if immune-ITH is linked to TME with different immunoselective pressure, which drives tumour evolution. Given the multistep nature of carcinogenesis and disease progression in HCC, it will be important to study and understand the evolution of its immune microenvironment along with tumour genomic evolution.

Our study aims to fill the knowledge gap in the field of tumour ITH and to examine the significance of immune-ITH in tumour evolution and disease progression. Using multi-sectoring and multi-omics approaches on different regions from a single HCC tumour, we found a marked degree of immune–ITH that was correlated to tumour transcriptomic-ITH. Concurrently, the overall TME showed decreasing immunoselective pressure with increased immune-ITH indicating an immune evolution towards immune exhaustion/suppression. Along with this differential immunoselective pressure, tumour evolved with distinct escape strategies. We also uncovered immune-ITH related transcriptome-immune networks and the distinct molecular pathways involved in dictating the disease progression and immune status. The current findings demonstrated the remodelling of immune landscape with increased immune-ITH as another dimension in tumour-immune co-evolution, which can be harnessed as a predictive signature for tumour progression.

Results

Significant degree of immune-ITH in HCC

Based on our previous discovery of significant genomic ITH and its impact on evolution trajectory in HCC[9], we aimed to examine the degree and implication of ITH in the immune landscapes from multiple regions within a HCC tumour. Following strict sampling protocol of two to five regions per tumour (**Supplementary Fig. 1a, b**), we prospectively collected a total of 95 tumour sectors (T), 28 adjacent non-tumour liver tissues N) and 28 peripheral blood (P) from 28 HCC patients who underwent surgical resection as the first-line therapy without any prior treatment (**Supplementary Table 1**). The samples from the same region were analysed by cytometry by time-of-flight (CyTOF) for their immunomic profile; as well as whole genome sequencing (WGS), and RNA-sequencing to examine the interrelationship between the immune profile with the genomic and transcriptomic profiles respectively (**Fig. 1a**). CyTOF analysis was performed using 38 surface or intracellular immune markers (**Supplementary Table 2**) as previously described[16].

First, we observed different level of ITH from the key immune lineages: B cells, CD8+ and CD4+ T cells, NK cells, NKT cells and macrophages. For instance, tumour sectors from patient B016 showed relatively homogeneous distributions of immune lineages whereas that from patient H255 show marked degree of ITH (**Fig. 1b**). Next, we focused on the ITH contributed by the major tumour-infiltrating leukocytes (TILs) subsets identified as the key global representative of TME in HCC from our previous study[16] (**Supplementary Fig. *2*a**). Indeed, we observed significant variations in the proportions (**Fig. 1c**) and the

variances (**Supplementary Fig. 2b**) of these 15 immune subsets in the TME of HCC, indicating marked degree of immune-ITH.

In order to validate if ITH was also reflected by tissue immune cell density, we next examined the heterogeneity in the densities of the $CD4^+$ and $CD8^+$ T cells within tumour tissues using multiplex-immunohistochemistry (mIHC). Indeed, we observed significant ITH of these T cells densities (**Fig. 1e**).

Taken together, the above data demonstrated significant immune–ITH within HCC tumours.

Immune-ITH correlated with tumour transcriptomic-ITH

Next, to systematically quantify for immune-ITH, we compared the proportions of these 15 immune subsets in pairwise manner across all tumour sectors from each single tumour using Spearman's correlation (rho), which measures degree of association or homogeneity[17]. The immune-ITH scores (degree of heterogeneity) were then reported as one minus rho **(Supplementary Fig. 3a**) and varying degrees of immune–ITH were identified for each tumour (**Fig. 2a** and **Supplementary Table 3**). We also calculated immune-ITH scores using Euclidean distance[18] and demonstrated a high correlation between the two scoring methods (rho= 0.99, **Fig. 2b)** resulting in the same immune-ITH groupings for the HCC tumours according to their respective medians (**Supplementary Fig. 4a**).

To further validate and correlate the immune-ITH between the immune cell proportions (CyTOF) and T cell densities (mIHC), we assigned ITH scoring to the T cell densities by calculating the standard deviation of $CD4^+$ and $CD8^+$ T cell densities from 10 regions for each tumour, reflecting its ITH. Indeed, we observed a significant correlation when comparing the degrees of immune-ITH based on CyTOF (proportions of immune subsets) or tissues mIHC (cell densities) (**Fig. 2c**), both demonstrating significant degree of Immune-ITH within the HCC tumours.

Next, we aimed to explore the relationship between immune-ITH with genomic- and transcriptomic-ITH, which were shown to be an important hallmark of tumour evolution[7, 9]. We calculated the tumour RNA-ITH, as 1 minus Spearman's rho for RNA expression of each gene and DNA–ITH, as ratio of the number of unique DNA mutations to the total number of DNA mutations, with references to previously described methods[9, 19] (**Supplementary Fig. 3b** and **Supplementary Table 3**). Comparing these ITHs, we found a strong correlation between immune–ITH and RNA–ITH (**Fig. 2d**), indicating a closer relationship between immune and tumour transcriptome landscapes. Instead, a weaker correlation between RNA-ITH and DNA-ITH and only a trend of positive correlation was observed between DNA-ITH and immune–ITH (**Fig. 2d**), suggesting that DNA–ITH (calculated based on all mutations) may have less impact or only certain specific DNA mutations may impact on immune-ITH.

As RNA-ITH is indicative of tumour evolution[7, 9], its correlation with immune-ITH provided evidence that increased immune-ITH could be a hallmark of immune evolution in HCC.

Immune exhaustive and suppressive TME in tumours with high immune-ITH

In order to underscore if immune-ITH has an impact on the overall immune status in tumours, we next compared the proportion of 15 key immune-subsets in these tumours. We found that tumours with high immune–ITH were significantly enriched with immunosuppressive/exhausted GB^- inactive memory $CD4^+$T cells, Treg and PD-1^+GB^- exhausted $CD8^+$-T cells; while conversely, tumours with low immune–ITH were enriched with activated/cytotoxic immune-subsets, such as $GB^+CD45RO^+$activated memory $CD4^+$-T cells, $CD69^{+/-}$NK cells, and GB^+PD-1^-activated $CD8^+$-T cells (**Fig. 3a**). This data demonstrated that apart from different immune-ITH, there was also distinct overall immune subsets distribution between tumours with low versus high immune-ITH. Additionally, we validated that the density of intratumoural Treg was indeed enriched in the tumours with high immune-ITH by tissue mIHC (**Fig.3b**). six other immune-subsets, including naïve $CD4^+$T cells and $CD14^+$macrophages, showed no significant enrichment in either tumour groups; although $CD27^-$ B cells with unknown functions, were also significantly enriched in tumours with low immune–ITH (**Fig. 3a** and **Supplementary Fig. 5a**).

Next, we also tested the functionality of $CD3^+$ T cells for cytokines production upon PMA/Ionomycin stimulation and observed varying percentages of cytokines-expressing T cells across different tumour sectors, demonstrating a marked degree of ITH in T cells functionality (**Fig. 3c**). Consistent with the findings above, the overall levels of the pro-inflammatory cytokines TNFa and IFNg in stimulated $CD3^+$ T cells were lower in tumours with high versus low immune–ITH (**Fig. 3d**).

Overall, tumours with low immune-ITH experienced stronger immune pressure; while tumours with higher immune-ITH harboured a more immunosuppressive and exhaustive TME. Such gradient towards immune inactivation with increased immune-ITH may indicate TME remodeling and evolution which could have important implications in tumour progression.

Tumour evolution events associated with tumours with different immune-ITH

As we hypothesized on the link between immune-ITH and tumour evolution, we next examined tumour evolution events such as tumour mutations, loss of heterozygosity in human leukocyte antigens (HLA-LOH) and immunoediting[14] with respect to immune-ITH. First, we observed higher events of copy number variations (CNVs), indicating higher genomic instability in tumours with high immune–ITH compared to those with low immune-ITH (**Fig. 4a**). Importantly, the total non-silent mutations were also higher in tumours with high immune-ITH (**Fig. 4b**), suggesting a tumour evolution trajectory with the accumulation of more mutational burden in tumours with higher immune-ITH. Next, we examined specific genomic mutations, namely the neoantigen (8-mer to 11-mer epitopes with <500 nM predicted binding affinity to

MHC-class 1), which could potentially be recognized by the immune system. Interestingly, tumours with high immune–ITH harboured higher total and subclonal (occurred in at least one but not all sectors), but not clonal (occurred in all sectors) neoantigens (**Fig. 4c**). This data suggests that the heterogeneity of neoantigens across tumour sectors represented by higher subclonal neoantigens mirrored that of the increased immune-ITH. Also since genomically heterogenous tumours with higher subclonal neoantigens was shown to be an indication of tumour evolution[20], this again provided evidence of potential co-evolution between the tumour and immune landscapes, where both demonstrated enhanced heterogeneity.

Given that the stronger immunoselective pressure experienced by tumours with lower immune-ITH could serve as a driving force for tumour escape mechanisms such as HLA-LOH and immunoediting[14], we next mapped the HLA-LOH and immunoediting (represented by the ratio of neoantigen/non-silent mutation) against immune-ITH from each tumour sector (**Fig. 4d)**. Interestingly, we observed lower immune–ITH in tumours with HLA-LOH (**Fig.4e)**, indicating a defective antigen-presentation machinery (HLA-LOH) was indeed a tumour escape mechanism in tumours with low immune-ITH**.** Additionally, we observed significant immunoediting (indicated by lower neoantigen/non-silent mutation ratio) only in tumours with low immune–ITH and intact HLA (**Fig.4f**); indicating that only tumours with stronger immune pressure (low immune-ITH) and antigen presentation capability (intact HLA) underwent immunoediting as another escape mechanism. We also confirmed this finding by calculating the immunoediting score as the ratio of observed:expected neoantigens per non-silent mutation according to previously published methods[14] (**Fig.4g**). This data once again strengthens the link between immune-ITH, immunoselective pressure and tumour escape mechanisms as a series of tumour evolutionary events.

Taken together, tumours with low immune-ITH that experienced higher immunoselective pressure underwent HLA-LOH and immunoediting as the intrinsic tumour escape mechanisms. Whereas tumours with high immune-ITH escaped with extrinsic mechanisms by remodeling towards a more immunoexhaustive and suppressive TME as well as accumulated more mutations particularly subclonal neoantigens. These distinct evolutionary mechanisms provided evidence for tumour and immune landscapes co-evolution along the gradient of immunoselective pressure and immune-ITH in HCC tumours.

Immune-ITH-related transcriptomic-immune network contributed to distinct tumour microenvironment

Given a significant correlation found between immune- and RNA-ITH (**Fig. 2d**), we next examined how the transcriptomic signatures is associated with immune-ITH or local immune activation status. We first identified a total of 1,709 differential expressed gene (DEGs) as the “immune-ITH transcriptomic signature” when comparing tumours with low versus high immune–ITH (**Supplementary Fig. 6a**). To further explore the interactions between the tumour-specific transcriptomic profile with its immune landscapes, we filtered off the genes contributed by immune subsets according to CIBERSORT[21] to

obtain the tumour-specific transcriptomes (n= 634 for low and n= 583 for high immune-ITH enriched DEGs, respectively). We then correlated these DEGs with the proportion of key immune-subsets in TME (from CyTOF) and constructed their respective transcriptome-immune networks specific to low or high immune-ITH. Interestingly, we found very distinct networks between low or high immune-ITH (**Fig 5a, b**). Low immune-ITH related tumour transcriptome showed positive association with cytotoxic NK cells and activated GB^{+}memory $CD4^{+}$ and PD-1^{-} GB^{+} $CD8^{+}$-T cells; or negative association with immunosuppressive Treg, exhausted PD-$1^{+}GB^{-}CD8^{+}$-T cells and inactive GB^{-}memory $CD4^{+}$-T cells (**Fig. 5a**). The opposite transcriptome-immune interactions were observed with high immune–ITH related transcriptomes, whereby positive correlations with immunosuppressive and exhaustive or negative correlations with cytotoxic and activated immune subsets were observed (**Fig. 5b**). These networks demonstrated that transcriptomic signature of high immune-ITH was closely linked to a immunosuppressive and exhausted TME, consistent with our data above.

Next we performed pathway enrichment analyses on these DEGs associated with these low or high immune-ITH networks (**Fig. 5c and Supplementary Table 4**) and found that metabolism pathway, particularly genes associated with fatty acid metabolism, such as *CPT2, ACAA2, CBR4, ECHDC2 and ACAA1* were positively associated with active $GB^{+}CD45RO^{+}$ memory $CD4^{+}$ and PD-$1^{-}GB^{+}CD8^{+}$ T cells (**Fig. 5a**). We also found a negative correlation between Treg and several glycoprotein-related genes such as *COL25A1, CLEC2B, CLEC1A, ADAMTS4, CLEC3B* and *ADAMTS1* (**Fig. 5a**), indicating the distinct metabolism pathways were potentially involved in maintaining the immune status of TME in HCC. Indeed, metabolic regulation of immune functions in cancer have been increasingly appreciated in a number of recent studies[22, 23].

Conversely, the pathways enriched in trancriptome-immune network from tumours with high immune-ITH included cell cycle, nucleotide-binding, centromere, microtubule and transcription, all of which were well known to be associated with tumour cell proliferation and disease progression[24, 25, 26]. Particularly, cell cycle genes such as *KIFC1*, *MCM7, MCM8, CSNK2A1* and *CDK19* that showed positive association with inactive $GB^{-}CD45RO^{+}$ resting $CD4^{+}$T cells and immunosuppressive Treg subsets or negative association with active PD-$1^{-}GB^{+}CD8^{+}$ T cells subset (**Fig. 5b**). Among which, KIFC1 was previously found to be a factor for poor prognostic and therapeutic target associated with tumour proliferation in HCC[27, 28], even though its immunodulatory function has never been described before. Another group of chaperone genes such as *CCT5, CCT7, CCT6A, CCT4, TCP1* and *PTGES3* showed negative correlation with active PD-1^{-} GB^{+}CD8+T cells (**Fig. 5b**). These cytosolic chaperone were previously implicated in cancer cell proliferation and predicts poor prognosis in HCC[29, 30].

The distinct gene-immune networks further strengthened the evidence that transcriptomic signature of immune-ITH was closely linked to the phenotypes of its TME. More importantly, it suggested that tumours with high immune-ITH demonstrated a transcriptomic network linked to immune exhaustion or suppression as well as tumour proliferation and disease progression.

High Immune–ITH predicts worse disease prognosis and survival in HCC patients

While genomic- and transcriptomic-ITH has been shown to correlate with poor prognosis in various cancers[31], the clinical relevance of immune–ITH remains unknown. Our data above suggest that tumours with high immune–ITH are more immunosuppressive, harbored more mutations and show aggressive or progressive tumour transcriptomic signature. By examining immune-ITH against multiple clinical parameters, we indeed found that high immune–ITH was associated with larger size of tumours, higher degree of fibrosis, the presence of microvascular invasion (MVI) and advanced TNM stage of tumour (**Fig. 6a, b**), all of which indicative of tumour progression and poor disease profiles. Of note, the immune-ITH is not associated with other parameters such as grade, viral status, AFP level or the number of tumour sectors harvested and analyzed (**Supplementary Fig. 7a**).

More importantly, patients with tumours of high immune–ITH had a significantly higher risk of recurrence than those with tumours of low immune–ITH (**Fig. 6c**). Of note, patients received no treatment prior to the point of recurrence, showing that this as a phenomenon following the natural trajectory of tumour evolution and disease progression that was not influenced by any therapeutic intervention. Next, we examined the survival impact of immune–ITH in our current cohort with both univariate and multivariate analyses, taking into consideration of multiple clinical factors including tumour stage, grade, size, MVI, as well as other factors associated with immune-ITH including cytokines-expressing $CD3^+$ T cells (representing TME immunoselective pressure), DNA- and RNA-ITH and tumour neoantigen burden. Among all the parameters, only immune-ITH as well as stage, tumour size, microvascular invasion (MVI) and race were significantly linked to RFS in the univariate analysis (**Supplementary Table 5**). From the multivariate analysis, we found that only immune–ITH remained an independent predictive factor for RFS, together with stage and MVI (**Fig. 6d**). Hence to rule out potential confounding effect from both stage and MVI, we tested the impact of immune-ITH only in patients with tumours from early stages (TNM stage I & II) or without MVI and found that immune-ITH remained an independent predictor of RFS (**Fig. 6e**). Taken together, increased immune-ITH was significantly associated with worse clinical profile and predicts for poor disease outcome in HCC patients.

Lastly, to validate the impact of immune-ITH on larger publicly available HCC dataset, we interrogated the expression profile of 1,709 immune–ITH gene signature in two large public HCC datasets: the Japanese Liver Cancer from the International Cancer Genome Consortium[32] (“Japanese”, n=203) and the Liver HCC from TCGA[33] (“TCGA”, n=315). For each dataset, we clustered the patients into low or high immune-ITH associated groups based on significant differential expression of immune-ITH related genes (**Supplementary Fig. 8a**). Indeed, we confirmed that patients with gene expression profiles resembling high immune–ITH had poorer overall survival (OS) than those with gene expression profiles resembling low immune–ITH, in both the Japanese and TCGA cohorts (1,000-time bootstrap FDR < 0.01, **Fig. 6f)**. Therefore, despite the fact that these publicly available transcriptomic data were obtained from single tumour biopsy, the molecular features underlying immune–ITH were consistently and closely linked to

advanced clinical trajectory. We further confirmed the robustness of our observations by shifting one patient between the immune–ITH groups and using leave-one (patient) out method to show that >95% of target genes remained consistent and capable of segregating patients' OS ($p < 0.01$; **Supplementary Fig. 8b,c**). Hence, we have identified and validated a robust immune–ITH signature capable of predicting disease prognosis in HCC patients.

In conclusion, we proposed a tumour-immune co-evolution model (**Fig. 6g**), where the immune landscapes evolved with increased immune-ITH and immunosuppressive/exhaustive TME; concurrently the tumours evolved with accumulation of more mutations and escaped using HLA-LOH or immunoediting. Collectively, these events lead to tumour progression and early recurrence, making immune-ITH a novel hallmark of tumour evolution and progression.

Discussion

The clinical relevance of immune-ITH and its relationship with tumour evolution were not explored previously. Our current study uncovered significant degree of immune-ITH from multiple HCC tumour regions and their inter-relationships with tumour evolution and impact on clinical outcome. We observed a significant degree of immune-ITH, which is linked to transcriptomic- or RNA-ITH. Importantly, a gradient of immunoselective pressure was uncovered along with immune-ITH and under this distinctive immunoselective pressure, the tumours employed distinct tumour escape mechanisms accordingly. The immune-ITH transcriptomic signature provided insights in pathways associated with tumour progression and dampening of immune response in TME. Lastly, our data demonstrated that immune-ITH correlated to worse clinical profile and could predict for poorer disease prognosis in HCC patients, emphasizing that immune–ITH as a hallmark of tumour evolution and critical indicator of disease progression. Taken together, our current findings suggest that the tumour and immune-microenvironments exhibit extensive cross-talk and co-evolve along tumour progression with increased immune-ITH, TME exhaustion and distinct tumour mutations, supporting a tumour-immune parallel evolution model (Fig. 6g).

It is important to appreciate that tumour-immune interaction is heterogeneous, dynamic and also bi-directional. For instance, immune pressure could potentially drive tumour genomic evolution[14, 34]; in return, immune landscapes are also constantly being shaped by the tumour transcriptomic landscapes[35, 36]. From our current data, the HCC TME shifted from homogenously "good" to heterogenously "bad" albeit exhausted and suppressive TME, forming a gradient of decreasing immunoselective pressure, an indication of immune landscape evolution. The tumours, on the other hand, accumulated more mutations especially subclonal neoantigens, showing its parallel evolution trajectory. Hence as concluded in the current study, the tumour-immune dynamic is changing constantly to adapt to one another, strengthening the concept of tumour-immune co-evolution championed by several previous studies[37]. Our findings also highlight that even within a single tumour, each tumour sector harbours its own unique mutation and microenvironment. This poses a notable challenge to conventional clinical decision-making, which is based on sampling of a single tumour biopsy. Despite a recent report that claimed the reliability of single-

sample in HCC from multi-region sampling and analysis using mainly IHC[38], our data proposed herein the existence of significant immune heterogeneity with clinical relevance with in-depth immuno-phenotyping pipeline.

Since both tumour mutational burden and TME have important implications in the response to immunotherapy[39, 40], higher total mutational burden, neoantigens loads as well as higher frequency of exhausted PD-1^{+}CD8^{+}-T cells, which are the prime target for anti-PD-1 immune-checkpoint blockade, in HCC tumours with high immune–ITH could potentially show better respond to immunotherapy. However, it must also be taken into consideration that these tumours are also infiltrated with more Treg and harboured higher subclonal neoantigen levels (consistent with a more heterogenous tumour), which may dampen the response and leading to resistance to immunotherapy[41, 42]. Moreover, the recent study from liver cancer patients treated with immune-checkpoint blockade demonstrated that low tumor transcriptomic diversity and higher cytolytic activity of CD8 + T cells, consistent with our tumours witn low immune-ITH, predicts clinical response to immunotherapy[6]. Therefore, it will be very important and interesting to study how this immune-ITH could affect response to immunotherapy with a deeper understanding of this intratumoural immune–host dynamics, which we believe would be helpful to stratify HCC patients for precision immunotherapy.

In conclusion, our study deciphers the complexity of intratumoural immune–host interaction and provides evidence showing immune-ITH as a novel hallmark of tumour-immune co-evolution along HCC progression.

Methods

Patients

95 tumour sectors from two to five regions per tumour (T), 28 matched adjacent non-tumour liver tissues (N) and pre-surgical blood were obtained fresh from 28 HCC patients underwent surgical resection at Singapore General Hospital, National Cancer Centre Singapore and National University Hospital **(Supplementary Table 1)**. Patient consent was obtained following each Institutional Review Board's guidelines. Patients received no pre or post-surgical treatment until recurrence, consistent with current standard of care. This allows us to study the natural progression of disease without the influence from treatment. Patients were monitored prospectively with regular imaging and other clinical investigations. Strict protocol of multi-sector tumour sampling was followed (**Supplementary Fig. 1a**,**b**) and each sector was divided for Mass Cytometry by Time-of-Flight (CyTOF), whole-genome sequencing (WGS) and RNA-sequencing (**Fig. 1a**). Tumour-infiltrating leukocytes (TILs) and non-tumour tissue-infiltrating leukocytes (NILs) were isolated by enzymatic digestion and peripheral blood mononuclear cells (PBMCs) by Ficoll-Paque layering as previously described[16].

CyTOF

CyTOF was performed as previously described[16]. Briefly, TILs, NILs and PBMCs were either unstimulated or stimulated with PMA and ionomycin (Sigma). Cells were processed and stained with 38 antibodies (**Supplementary Table 2**) purchased preconjugated or conjugated in-house according to the manufacturer's instructions (Fluidigm) before analysis on a Helios^{TM}mass-cytometer (Fluidigm). The generated files were analysed using FlowJo (v.10.2; FlowJo) as previously described [43].

ITH quantification and immunohistochemistry (IHC)

15-immune subsets were manually gated (**Supplementary Fig. 2a**) and the proportions in each tumour sector were calculated. The ITH scores were calculated with reference to previously described methods[9, 19] for patients with ≥2 tumour sectors using pairwise comparison of all sectors for: (i) DNA, as ratio of the number of unique DNA mutations to the total number of DNA mutations; (ii) RNA, as 1 minus the Spearman correlation coefficient's Rho of RNA expression of each gene; and (iii) immune, as 1 minus the Spearman's Rho of proportions of the 15 immune subsets. The median values were taken as the patient-level ITH scores.

Multiplex IHC on representative formalin-fixed paraffin-embedded tissues (n=26), was performed as previously described[44] with anti-human CD4 (Abcam, clone EPR6855, 1:200) and CD8 (DAKO, clone C8/144B, 1:200) antibodies. The density of $CD4^+$ and $CD8^+$ was quantified as number of cells/mm^2 from 10 3mm^2 representative fields. We then calculated the standard deviation of cell density across tumour regions, which reflects the heterogeneity or similarity, for each tumour. The degree of fibrosis were also scored according to Metavir scoring system[45] using standard H&E staining on the adjacent non-tumour liver tissue sections.

RNA sequencing

Total RNAs were isolated from tissues using Picopure RNA-Isolation kit (Arcuturus, Ambion) and cDNAs constructed using SMART-Seq®v4 UltraTM Low Input RNA Kit (Clontech, USA). Illumina-indexed libraries were generated using Nextera-XT DNA-Library Prep Kit (Illumina, USA). RNA sequencing was performed on HiSeq High output platform at the Genome Institute of Singapore (GIS).

The raw reads were aligned via STAR[46] to the Human Reference Genome hg19 and the expected gene-level counts were calculated using RSEM[47]. Only protein-coding genes with >1 count/million reads in ³5% of the samples were retained. Data were normalized using DEseq2 and differentially expressed genes (DEGs) analysis was performed using the R package Limma[48] at false discovery rate (FDR)<0.01. Pathway enrichment analyses were performed using DAVIDv6.8. For RNA-immune network and

correlation analyses, genes from immune subsets were filtered out according to the gene list provided by CIBERSORT [21] and were performed using ggplot2 for selected DEGs with $p<0.05$ and $rho \geq 0.4$.

Whole genome sequencing (WGS)

WGS was performed as previously described[9]. Briefly, DNA was extracted from tissues using Qiagen AllPrep kit, DNA fragments were end-repaired, ligated with sequencing adapters, amplified, and sequenced by Illumina sequencing platform at GIS. Raw reads were mapped to the Human Reference Genome hg19 using Burrows–Wheeler Aligner. Duplicated reads were removed, base-quality recalibration and realignment were performed. Somatic variants were called by comparing tumour versus non-tumour samples using Mutect (v1.1.4)[49].

Copy number variation (CNV) analysis and Non-silent mutations

Somatic CNVs were called and segmented with Sequenza. Gene-level copy-numbers were obtained with GISTIC(v2.0) using segmented copy numbers[50]. Altered genome fraction was calculated by considering the segments with integer copy number greater or less than the median copy number. The fraction was calculated as total length of aberrant segments/total length of all segments. To compare the altered genome fractions in two immune ITH groups, a two-sided Wilcoxon rank sum test was used. The CNV frequency differences were identified by comparing the cytoband level copy numbers between two immune–ITH groups using Fisher's exact test with adjusted Benjamini-Hochberg p-values.

Non-silent or nonsynonymous mutations were computed from mutations resulting in both missense (mutations in a single nucleotide that result in alternation in amino acid encoded) and nonsense (mutations in the DNA sequence resulting in a stop codon) mutations[49].

Loss of heterozygosity in human leukocyte antigens (HLA-LOH) analysis, Neoantigen prediction and immunoediting scoring

MHC class I: HLA-A, -B, -C genes were determined by Polysolver[51], purity and ploidy values by Sequenza[52] and HLA copy-number calling by LOHHLA[53]. Minor allele copy number<0.5 was considered as HLA-LOH. Neoantigen prediction was performed using personalized Variant Antigens by Cancer Sequencing(pVacSeq)[54], and variants calling information were obtained from MuTect[49]. The variant calls were annotated using VEP: 8- to 11-mer epitopes with <500 nM binding affinity. Total, clonal (expressed by all tumour sectors) and subclonal (expressed by at least one but not all sectors) neoantigens were computed. The immunoediting scores were computed as the ratio of observed neoantigen/expected

mutations as previously described[14]. Briefly, the expected number of non-silent mutations and neo-peptides were calculated based on mutational spectra estimated empirically[14] and compared to the observed number of non-silent mutations and neoantigens.

Survival analysis

Kaplan Meier analysis of recurrence-free survival (RFS) was performed with the log-rank (ManteleCox) test (GraphPad Prism v7.0b). Univariate and multivariate analyses were performed using Cox proportional hazards model.

Two public HCC datasets were analysed to assess the survival impact of the immune–ITH (using n=1,709 DEGs) and FDR was estimated by 1,000-time bootstrap. Specifically, we segregated the patients based on the differential expression level of 1,709 DEGs associated with immune-ITH from our current cohort; i.e. the patients showing high expression of low-immune-ITH associated genes was grouped as low-immune-ITH group and those with high expression of high-immune-ITH associated genes was grouped as high immune-ITH group (**Supplementary Fig. 8a**). We then examined the survival profile between these two groups of patients by Kaplan Meier. The raw counts for the Japanese Liver Cancer from the International Cancer Genome Consortium (Liver Cancer-RIKEN, Japan; Project Code LIRI-JP) and the TCGA dataset (Liver HCC, The Cancer Genome Atlas) were downloaded from the International Cancer Genome Consortium Data Portal[32] and FireBrowse[33], respectively. Only protein-coding genes with FPKM >1 (Japanese dataset) or raw counts >1 (TCGA dataset) in ³5 samples were retained and data were normalized using DEseq2.

Declarations

Acknowledgements

The authors would like to thank all members of TII, all participating patients, the clinical research coordinators from NCCS, SGH, NUHS for their contributions and Insight Editing London for language editing of this manuscript. This work was supported by the National Medical Research Council (NMRC), Singapore (ref numbers: TCR15Jun006, CIRG16may048, CSAS16Nov006, CSASI17may003, LCG17MAY003, NMRC/STaR/020/2013, NMRC/CG/M003/2017, LCG17MAY004 and NMRC/OFIRG/0064/2017) and National Research Foundation, Singapore (ref number: NRF-NRFF2015-04). We thank all the patients who participate in The PLANET study- a prospective cohort study on the impact of intra-tumoral genomic heterogeneity on the clinical trajectory of resected HCC (https://clinicaltrials.gov/ct2/show/NCT03267641).

References

1. Sanyal AJ, Yoon SK, Lencioni R. The etiology of hepatocellular carcinoma and consequences for treatment. *Oncologist* **15 Suppl 4**, 14–22 (2010).
2. Bray F, Ferlay J, Soerjomataram I, Siegel RL, Torre LA, Jemal A. Global cancer statistics 2018: GLOBOCAN estimates of incidence and mortality worldwide for 36 cancers in 185 countries. *CA Cancer J Clin* **68**, 394–424 (2018).
3. El-Khoueiry AB, *et al.* Nivolumab in patients with advanced hepatocellular carcinoma (CheckMate 040): an open-label, non-comparative, phase 1/2 dose escalation and expansion trial. *Lancet* **389**, 2492–2502 (2017).
4. Zhu AX, *et al.* Pembrolizumab in patients with advanced hepatocellular carcinoma previously treated with sorafenib (KEYNOTE-224): a non-randomised, open-label phase 2 trial. *Lancet Oncol* **19**, 940–952 (2018).
5. A-L. Cheng SQ, M. Ikeda, P. Galle, M. Ducreux, A. Zhu, T-Y. Kim, M. Kudo, V. Breder, P. Merle, A. Kaseb, D. Li, W. Verret, Z. Xu, S. Hernandez, J. Liu, C. Huang, S. Mulla, H.Y. Lim, R. Finn. Abstract LBA3 - IMbrave150: Efficacy and safety results from a ph III study evaluating atezolizumab (atezo) + bevacizumab (bev) vs sorafenib (Sor) as first treatment (tx) for patients (pts) with unresectable hepatocellular carcinoma (HCC). *Annals of Oncology* **30**, (2019).
6. Ma L, *et al.* Tumor Cell Biodiversity Drives Microenvironmental Reprogramming in Liver Cancer. *Cancer Cell* **36**, 418–430 e416 (2019).
7. de Bruin EC, *et al.* Spatial and temporal diversity in genomic instability processes defines lung cancer evolution. *Science* **346**, 251–256 (2014).
8. Xue R, *et al.* Variable Intra-Tumor Genomic Heterogeneity of Multiple Lesions in Patients With Hepatocellular Carcinoma. *Gastroenterology* **150**, 998–1008 (2016).
9. Zhai W, *et al.* The spatial organization of intra-tumour heterogeneity and evolutionary trajectories of metastases in hepatocellular carcinoma. *Nat Commun* **8**, 4565 (2017).
10. Zhang Q LY, Yang J, et al. Integrated multiomic analysis reveals comprehensive tumour heterogeneity and novel immunophenotypic classification in hepatocellular carcinomas. *Gut* **Published Online First**: **21 June** 2019., (2019).
11. Zhang AW, *et al.* Interfaces of Malignant and Immunologic Clonal Dynamics in Ovarian Cancer. *Cell* **173**, 1755–1769 e1722 (2018).
12. Losic B, *et al.* Intratumoral heterogeneity and clonal evolution in liver cancer. *Nat Commun* **11**, 291 (2020).
13. Angelova M, *et al.* Evolution of Metastases in Space and Time under Immune Selection. *Cell* **175**, 751–765 e716 (2018).
14. Rooney MS, Shukla SA, Wu CJ, Getz G, Hacohen N. Molecular and genetic properties of tumors associated with local immune cytolytic activity. *Cell* **160**, 48–61 (2015).
15. Jimenez-Sanchez A, *et al.* Heterogeneous Tumor-Immune Microenvironments among Differentially Growing Metastases in an Ovarian Cancer Patient. *Cell* **170**, 927–938 e920 (2017).

16. Chew V, *et al.* Delineation of an immunosuppressive gradient in hepatocellular carcinoma using high-dimensional proteomic and transcriptomic analyses. *Proc Natl Acad Sci U S A* **114**, E5900-E5909 (2017).
17. Spearman C. The proof and measurement of association between two things. By C. Spearman, 1904. *Am J Psychol* **100**, 441–471 (1987).
18. Rosenthal R, *et al.* Neoantigen-directed immune escape in lung cancer evolution. *Nature*, (2019).
19. Jiang T, *et al.* Statistical measures of transcriptional diversity capture genomic heterogeneity of cancer. *BMC Genomics* **15**, 876 (2014).
20. McGranahan N, Swanton C. Clonal Heterogeneity and Tumor Evolution: Past, Present, and the Future. *Cell* **168**, 613–628 (2017).
21. Newman AM, *et al.* Robust enumeration of cell subsets from tissue expression profiles. *Nat Methods* **12**, 453–457 (2015).
22. Ngwa VM, Edwards DN, Philip M, Chen J. Microenvironmental Metabolism Regulates Antitumor Immunity. *Cancer Res* **79**, 4003–4008 (2019).
23. Chang CH, *et al.* Metabolic Competition in the Tumor Microenvironment Is a Driver of Cancer Progression. *Cell* **162**, 1229–1241 (2015).
24. Hanahan D, Weinberg RA. The hallmarks of cancer. *Cell* **100**, 57–70 (2000).
25. Bradner JE, Hnisz D, Young RA. Transcriptional Addiction in Cancer. *Cell* **168**, 629–643 (2017).
26. Collins K, Jacks T, Pavletich NP. The cell cycle and cancer. *Proc Natl Acad Sci U S A* **94**, 2776–2778 (1997).
27. Wang X, Wang M, Li XY, Li J, Zhao DP. KIFC1 promotes the proliferation of hepatocellular carcinoma in vitro and in vivo. *Oncol Lett* **18**, 5739–5746 (2019).
28. Fu X, *et al.* KIFC1, a novel potential prognostic factor and therapeutic target in hepatocellular carcinoma. *Int J Oncol* **52**, 1912–1922 (2018).
29. Boudiaf-Benmammar C, Cresteil T, Melki R. The cytosolic chaperonin CCT/TRiC and cancer cell proliferation. *PLoS One* **8**, e60895 (2013).
30. Cui X, Hu ZP, Li Z, Gao PJ, Zhu JY. Overexpression of chaperonin containing TCP1, subunit 3 predicts poor prognosis in hepatocellular carcinoma. *World J Gastroenterol* **21**, 8588–8604 (2015).
31. McGranahan N, Swanton C. Biological and therapeutic impact of intratumor heterogeneity in cancer evolution. *Cancer Cell* **27**, 15–26 (2015).
32. Zhang J, *et al.* International Cancer Genome Consortium Data Portal–a one-stop shop for cancer genomics data. *Database (Oxford)* 2011, bar026 (2011).
33. Cancer Genome Atlas Research N, *et al.* The Cancer Genome Atlas Pan-Cancer analysis project. *Nat Genet* **45**, 1113–1120 (2013).
34. Jamal-Hanjani M, Quezada SA, Larkin J, Swanton C. Translational implications of tumor heterogeneity. *Clin Cancer Res* **21**, 1258–1266 (2015).
35. Thorsson V, *et al.* The Immune Landscape of Cancer. *Immunity* **48**, 812–830 e814 (2018).

36. Zerdes I, Matikas A, Bergh J, Rassidakis GZ, Foukakis T. Genetic, transcriptional and post-translational regulation of the programmed death protein ligand 1 in cancer: biology and clinical correlations. *Oncogene* **37**, 4639–4661 (2018).
37. Galon J, Bruni D. Tumor Immunology and Tumor Evolution: Intertwined Histories. *Immunity* **52**, 55–81 (2020).
38. Shen YC, *et al.* Reliability of a Single-region Sample to evaluate Immune Tumor Microenvironment in Hepatocellular Carcinoma. *J Hepatol*, (2019).
39. Rizvi NA, *et al.* Cancer immunology. Mutational landscape determines sensitivity to PD-1 blockade in non-small cell lung cancer. *Science* **348**, 124–128 (2015).
40. Thommen DS, *et al.* A transcriptionally and functionally distinct PD-1(+) CD8(+) T cell pool with predictive potential in non-small-cell lung cancer treated with PD-1 blockade. *Nat Med* **24**, 994–1004 (2018).
41. McGranahan N, *et al.* Clonal neoantigens elicit T cell immunoreactivity and sensitivity to immune checkpoint blockade. *Science* **351**, 1463–1469 (2016).
42. Tanaka A, Sakaguchi S. Regulatory T cells in cancer immunotherapy. *Cell Res* **27**, 109–118 (2017).
43. Chew V, *et al.* Immune activation underlies a sustained clinical response to Yttrium-90 radioembolisation in hepatocellular carcinoma. *Gut*, (2018).
44. Garnelo M, *et al.* Interaction between tumour-infiltrating B cells and T cells controls the progression of hepatocellular carcinoma. *Gut* **66**, 342–351 (2017).
45. Goodman ZD. Grading and staging systems for inflammation and fibrosis in chronic liver diseases. *J Hepatol* **47**, 598–607 (2007).
46. Dobin A, *et al.* STAR: ultrafast universal RNA-seq aligner. *Bioinformatics* **29**, 15–21 (2013).
47. Li B, Dewey CN. RSEM: accurate transcript quantification from RNA-Seq data with or without a reference genome. *BMC Bioinformatics* **12**, 323 (2011).
48. Smyth GK. *Limma: linear models for microarray data*. Springer (2005).
49. Cibulskis K, *et al.* Sensitive detection of somatic point mutations in impure and heterogeneous cancer samples. *Nat Biotechnol* **31**, 213–219 (2013).
50. Mermel CH, Schumacher SE, Hill B, Meyerson ML, Beroukhim R, Getz G. GISTIC2.0 facilitates sensitive and confident localization of the targets of focal somatic copy-number alteration in human cancers. *Genome Biol* **12**, R41 (2011).
51. Shukla SA, *et al.* Comprehensive analysis of cancer-associated somatic mutations in class I HLA genes. *Nat Biotechnol* **33**, 1152–1158 (2015).
52. Favero F, *et al.* Sequenza: allele-specific copy number and mutation profiles from tumor sequencing data. *Ann Oncol* **26**, 64–70 (2015).
53. McGranahan N, *et al.* Allele-Specific HLA Loss and Immune Escape in Lung Cancer Evolution. *Cell* **171**, 1259–1271 e1211 (2017).

54. Hundal J, *et al.* pVAC-Seq: A genome-guided in silico approach to identifying tumor neoantigens. *Genome Med* **8**, 11 (2016).

Abbreviations

CyTOF, mass Cytometry by Time-of-Flight; DEGs, differentially expressed genes; FDR, false discovery rate; GB, granzyme-B; HCC, hepatocellular carcinoma; HLA-LOH, loss of heterozygosity in human leukocyte antigens; HR, Hazard ratio; ITH, intratumoural heterogeneity; MVI, microvascular invasion; NK, natural killer; PBMCs, peripheral blood mononuclear cells; RFS, recurrence-free survival; TCGA, the Liver Hepatocellular Carcinoma from The Cancer Genome Atlas, TILs, tumour-infiltrating leukocytes; TME, tumour microenvironment; Treg, regulatory T cells; WGS, whole genome sequencing; PMA, phorbol myristate acetate

Declarations

Conflict of interest statement: The authors declare no conflicts of interest

Financial support statement: This work was supported by the National Medical Research Council (NMRC), Singapore (ref numbers: TCR15Jun006, CIRG16may048, CSAS16Nov006, CSASI17may003, LCG17MAY003, NMRC/STaR/020/2013, NMRC/CG/M003/2017, LCG17MAY004 and NMRC/OFIRG/0064/2017) and National Research Foundation, Singapore (ref number: NRF-NRFF2015-04).

Author contributions P.N. obtained and analysed data and prepared the paper; S.M. obtained and analysed the genomic/transcriptomic data and prepared the paper. C.P., N.K. and H.L. analysed the genomic/transcriptomic data. C.J.L. and J.Q.L. processed the samples and performed experiments. L.L. provided technical help with CyTOF and performed experiments. W.L.T. provided genomic/transcriptomic analysis support. T.K.H.L., W.K.W., T.L., W.Q.L. and P.Y.H. prepared and provided tissue samples and discussed the data. C.Y.C., S.Y.L., P.C.C., H.C.T., S.I., A.K., Y.Y. D., A.C. and B.K.P.G. recruited patients, provided samples and discussed the data. F.G. provided analysis support for immunomics data. S.A. designed the CyTOF pipeline and discussed the data. P.K.H.C. initiated the project, provided patient samples and discussed the data; W.Z. designed and led the genomics analysis and prepared the paper; V.C. designed and led the study, performed the immunomics analysis and prepared the paper.

Figures

Fig. 1.

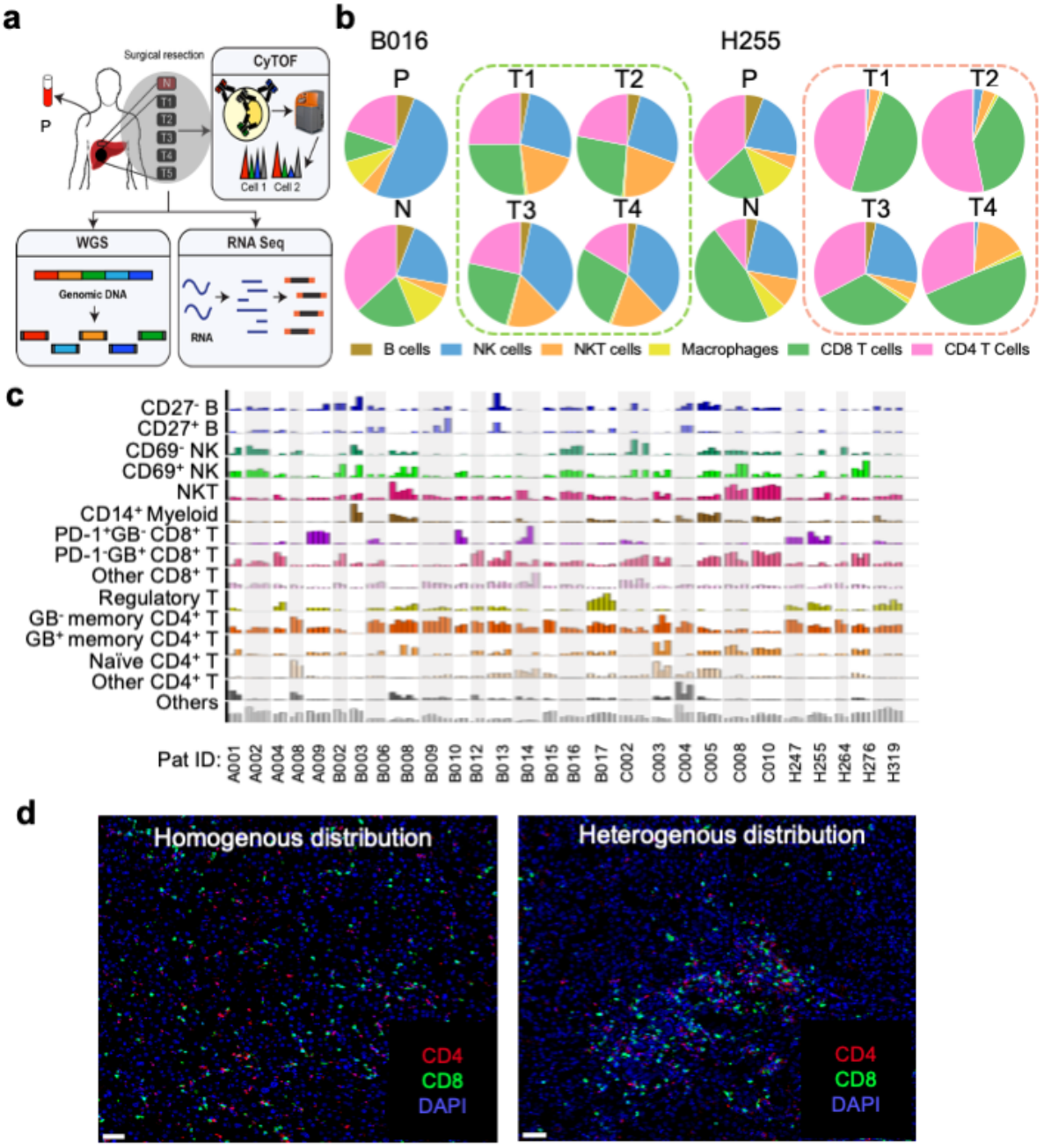

Figure 1

Significant degree of intratumoural heterogeneity (ITH) in the immune landscapes of HCC. a Two to five tumour sectors (T), one adjacent non-tumour sector (N) and one PBMC (P) sample was harvested from each HCC patient and analysed by CyTOF, RNA sequencing (seq) or whole genome sequencing (WGS) for their genomic, transcriptomic and immunomic profiles. b Pie charts showing the proportions of major immune lineages in P, N and T sectors from representative tumours showing low (Patient B016) or high

(Patient H255) immune-ITH. c Bar graphs showing proportions of 15 immune subsets (percentages of each immune subsets of total live CD45+ immune cells) in 28 HCC patients (labelled and separated by grey colour zone). d Representative images from multiplex immunohistochemistry (mIHC) stained for CD8 (green), CD4 (red), and DAPI (blue) on either homogenous (patient A002) or heterogeneous (patient C002) tumours. Scale bar, 50 μm.

Fig. 2.

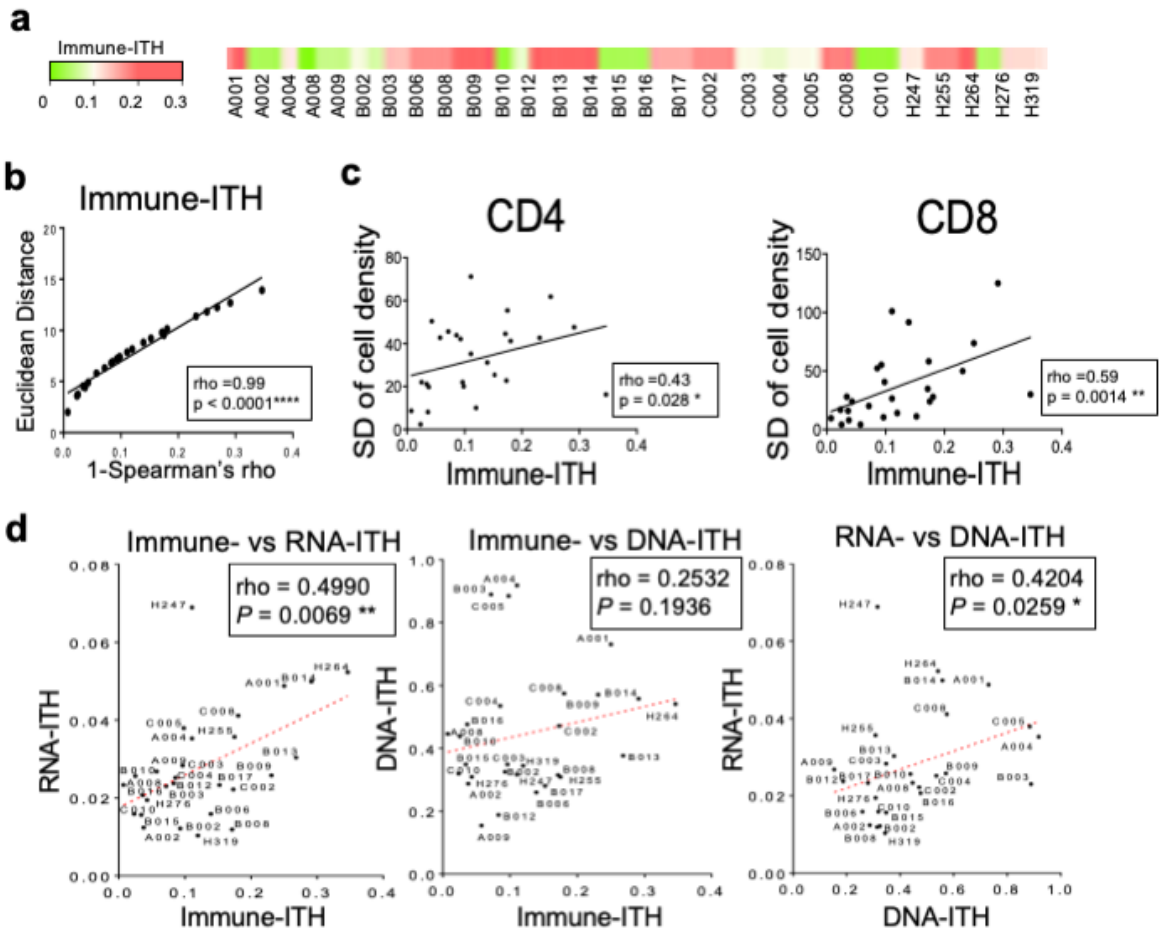

Figure 2

Immune intratumoural heterogeneity (ITH) quantification and correlation with RNA- and DNA-ITH a Heatmap showing relative immune–ITH scores of 28 HCC patients with respect to its median value at 0.10446. Each bar represents a single tumour sector. b Scatter plot for correlation between immune-ITH scores by Spearman's correlation and Euclidian distance metrics. c Correlation between immune-ITH calculated from CyTOF data by Spearson's correlation and standard deviation (SD) of CD4+ and CD8+ T-cell density. d Correlation of ITH between immune, RNA (transcriptomic) and DNA (genomics) profiles. b-d Spearman's correlation coefficient, rho and p value were indicated.

Fig. 3.

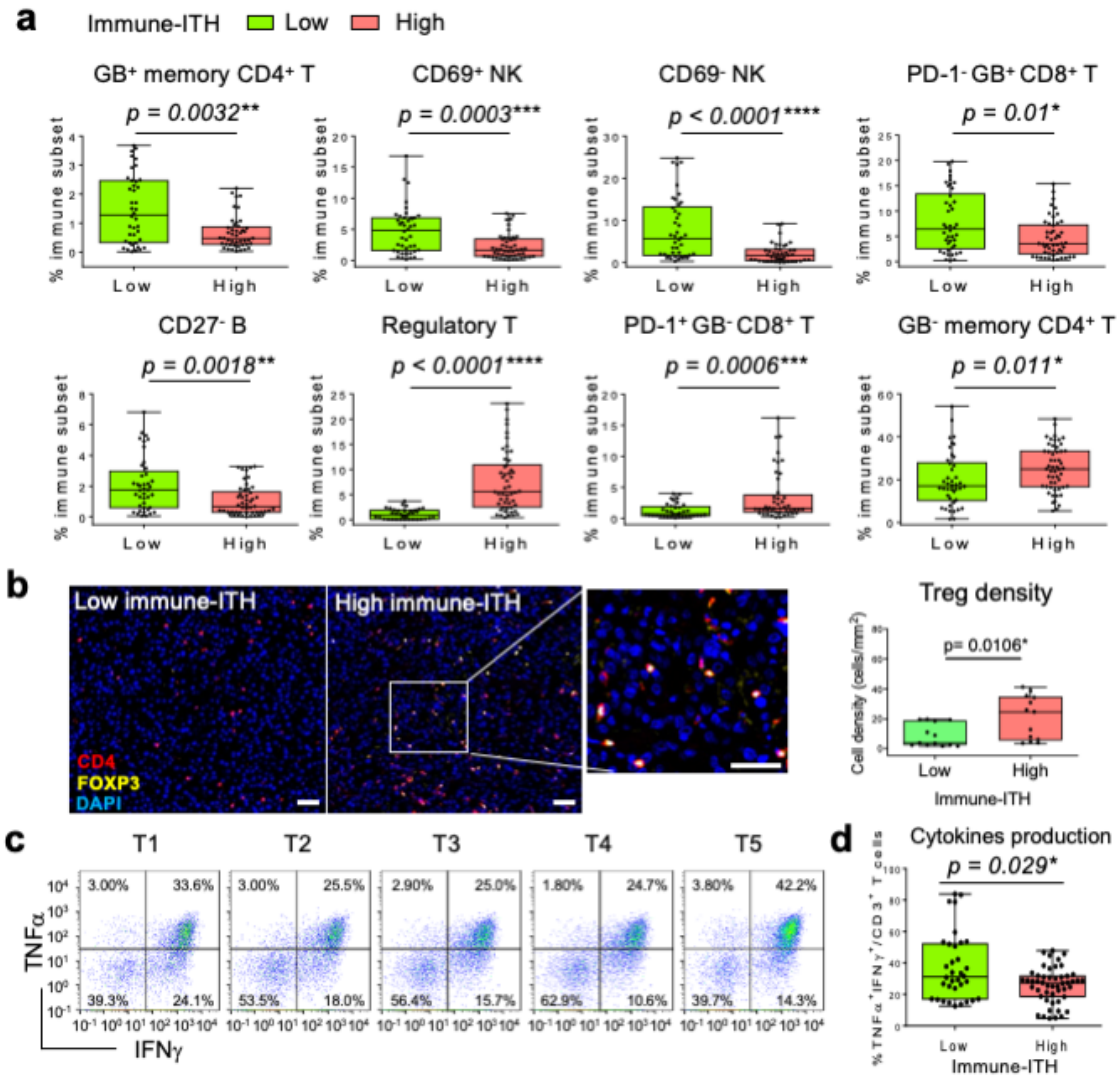

Figure 3

Differential immunoselective pressure in tumours with low versus high immune–intratumoural heterogeneity (ITH). a Immune subsets that were significantly enriched in tumours with low versus high immune–ITH. b Left, representative multiplex immunohistochemistry (mIHC) images stained for CD4 (red), Foxp3 (yellow) and DAPI (blue) on tumour tissues with low (patient B016) or high (patient H319) immune-ITH. Scale bar, 50 μm. Right, Treg cell density (count/mm2) in tumours with low versus high immune-ITH. c Dot plots showing percentages of intracellular pro-inflammatory cytokines IFN and TNF in CD3+ T cells from T1 to T5 tumour sectors of representative Patient H319. d Percentage of TNF and IFN-expressing CD3+ T cells in tumours with low and high immune–ITH. Cells were stimulated with PMA/Ionomycin for 5h. a, b and d, Data was shown by box plot. The whiskers represent minimum and maximum values, the band inside the box is the median and box edges show the first and third quartiles. *P < 0.05, ** P < 0.01, ***P < 0.001, ****P < 0.0001 by two-sided Mann-Whitney U-test.

Fig. 4.

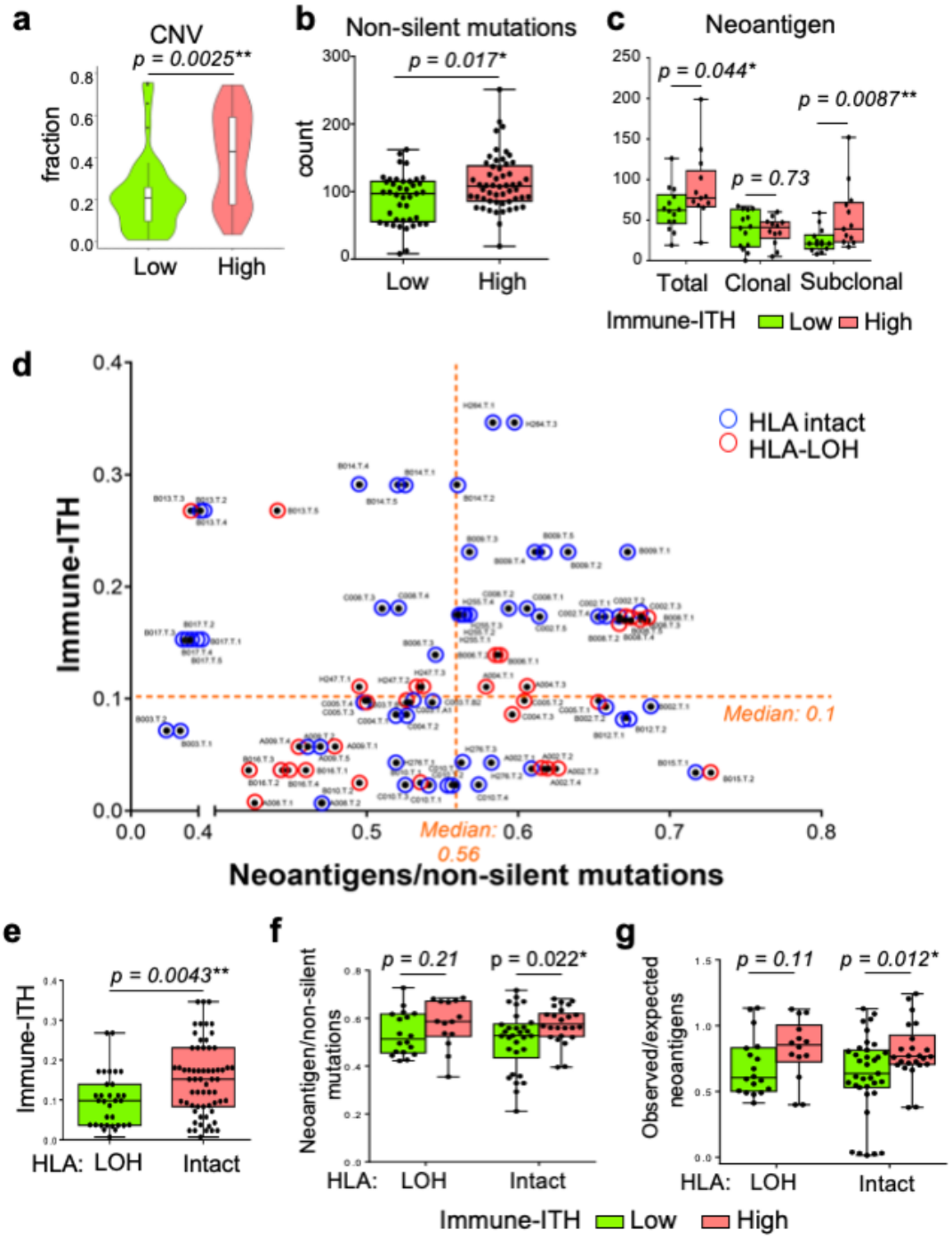

Figure 4

Significant HLA-LOH and immunoediting in tumours with low immune-ITH a Copy number variations (CNV) calculated based on altered genome fractions in low versus high immune–ITH tumours. **P < 0.01 by Two-sided Wilcoxon rank sum test. b Total non-silent mutational load in high versus low immune–ITH tumours. c Total, clonal and subclonal neoantigen loads in low versus high immune–ITH tumours. d Immune-ITH scores of each HCC tumour sector were plotted against its neoantigen/non-silent mutations

ratio, which is indicative of immunoediting. Orange dash line denotes median level of immune-ITH or median of neoantigen/non-silent mutations, as indicated respectively. Red circles show tumours with HLA-LOH event and blue circles show intact HLA. e Immune–ITH scores in tumours with or without HLA-LOH. f Ratio of neoantigen over non-silent mutation and g ratio of observed:expected neoantigen in high versus low immune–ITH tumours with or without HLA-LOH. (a-c and e-g) Data was shown by box plot. The whiskers represent minimum and maximum values, the band inside the box is the median and box edges show the first and third quartiles. *P < 0.05 or ** P < 0.01 by two-sided Mann-Whitney U-test.

Fig. 5.

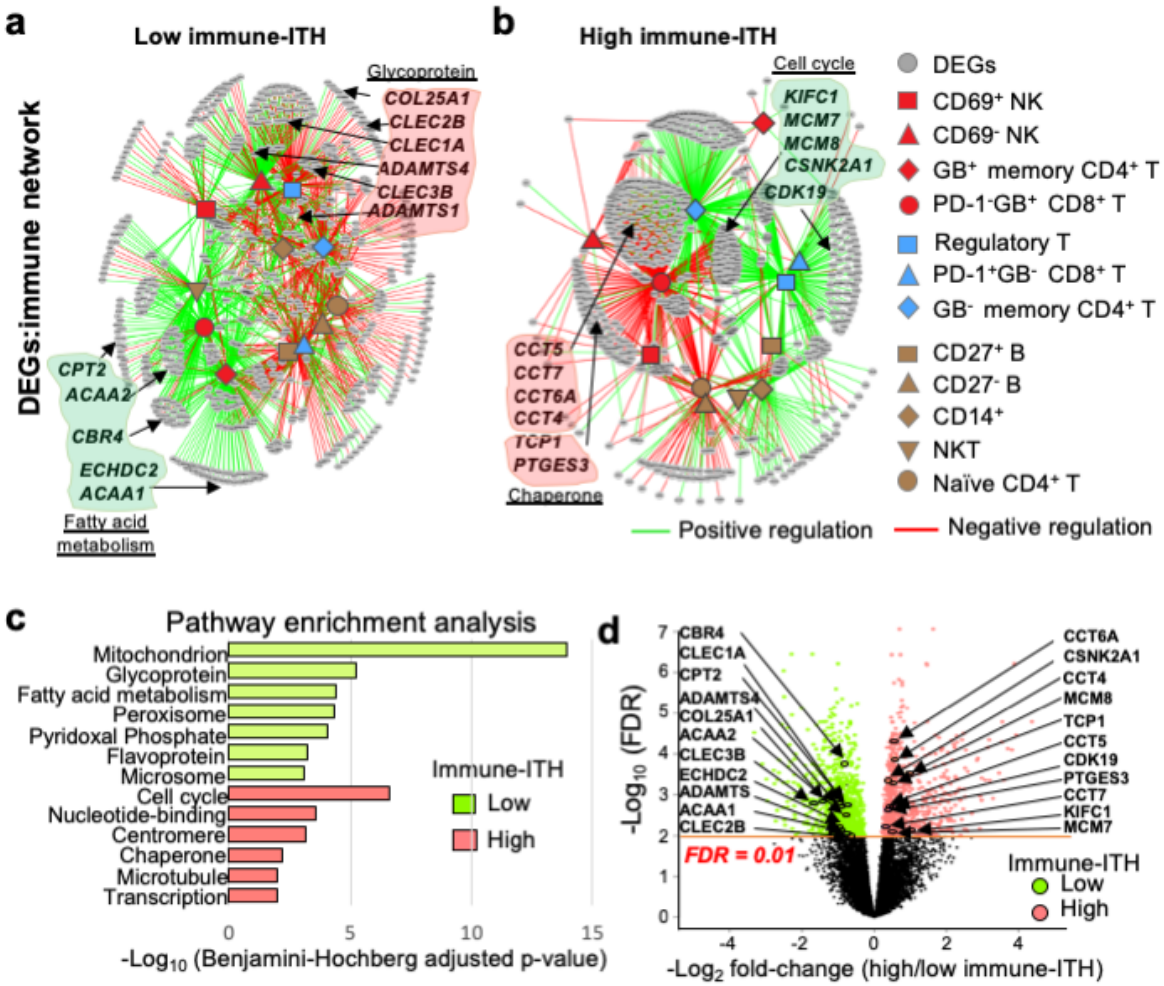

Figure 5

Transcriptome-immune networks associated with immune–intratumoural heterogeneity (ITH). a and b Transcriptome-immune network showing correlation between the immune subsets and the tumour transcriptome associated with a low or b high immune–ITH. Green and red lines denote positive and negative correlation, respectively (Spearman's correlation test, rho ≥ 0.4, P < 0.05). The immune subsets are denoted as Red: cytotoxic/activated; Blue: immunosuppressive/exhausted; and brown: controversial roles. b DAVID pathway enrichment analysis of the genes enriched in tumours with low or high immune–ITH. c Volcano plot showing DEGs with selected genes as highlighted in the low and high immune–ITH tumours. The orange line denotes the false discovery rate (FDR) = 0.01.

Fig. 6.

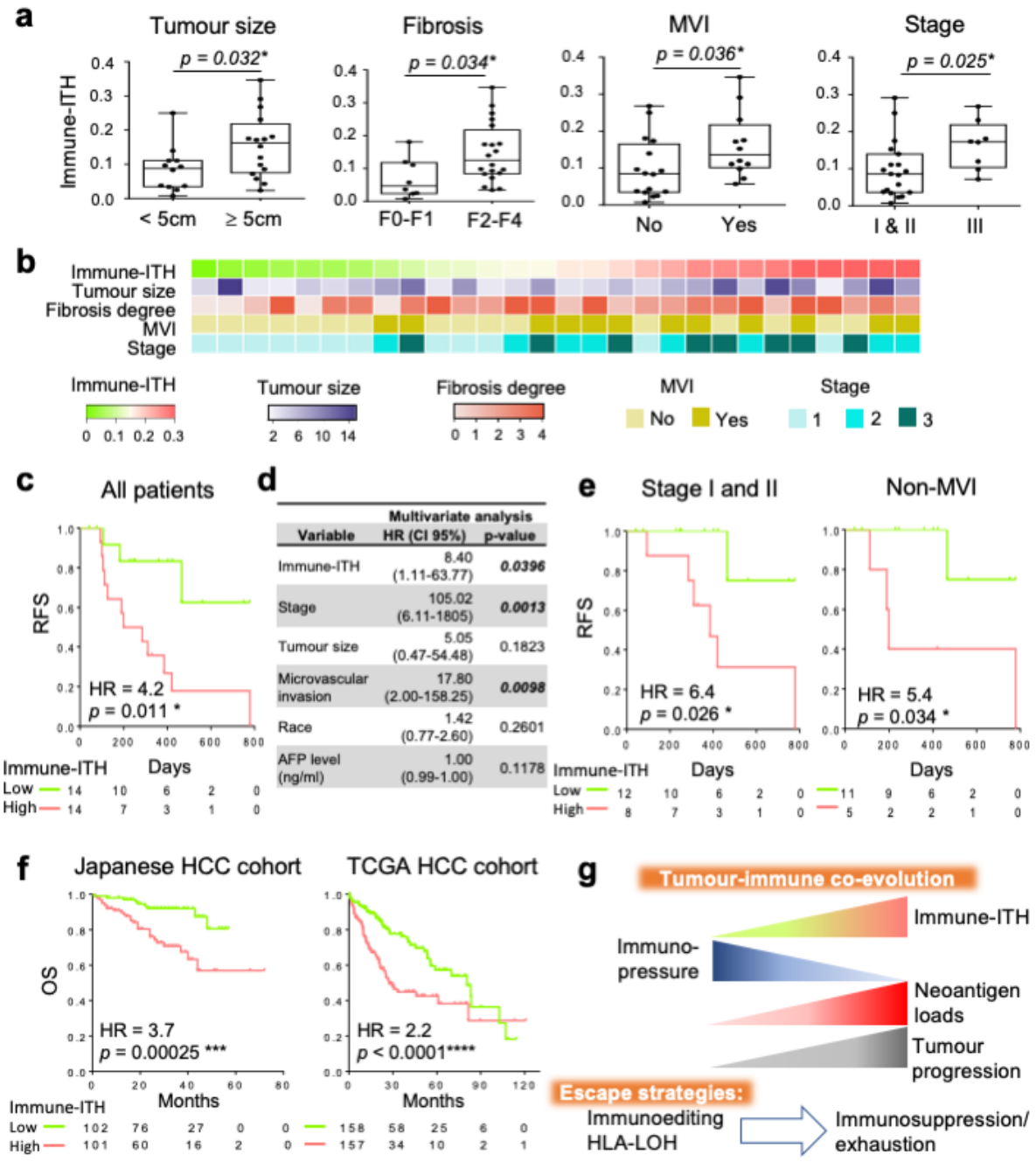

Figure 6

High immune–intratumoural heterogeneity (ITH) is associated with poor patient clinical outcome a Immune–ITH in tumours: <5cm versus ≥5cm (size based on Milan criteria); low (F0-F1) versus high (F2-F4) fibrosis stage (METAVIR scoring system), without or with presence of microvascular invasion (MVI) and early (stage I & II) versus late (Stage III) stage (TNM version 8). Data was shown by box plot. The whiskers represent minimum and maximum values, the band inside the box is the median and box edges

show the first and third quartiles. *P < 0.05 by two-sided Mann-Whitney U-test. b Heatmaps showing immune-ITH, tumour size (cm), microvascular invasion (Yes as present; no as absent) and Stage (TNM version 8) from 28 patients. c Kaplan-Meier curves for recurrence-free survival (RFS) profiles of 28 HCC patients with low or high immune–ITH tumours. d Multivariate analysis of clinical and biological variables using Cox proportional hazards regression models. e Kaplan-Meier curves for RFS profiles of patients with tumours from early stages or without MVI segregated by low or high immune–ITH tumours. f Kaplan-Meier curves for overall survival (OS) profiles of Japanese (n=203) and TCGA cohorts (n= 315) segregated DEGs associated with immune–ITH. Kaplan-Meier graphs showing immune-ITH low (green) or high (red); Hazard ratio (HR) and logrank test P values as indicated. c, e and f Kaplan-Meier graphs showing immune-ITH low (green) or high (red); Hazard ratio (HR) and logrank test P values as indicated. g A graphical summary of tumour-immune co-evolution model with distinct tumour escape strategies.